



Research papers

A blueprint for adapting high Aswan dam operation in Egypt to challenges of filling and operation of the Grand Ethiopian Renaissance dam

Hisham Eldardiry, Faisal Hossain *

Department of Civil and Environmental Engineering, University of Washington, Seattle, United States

Nomenclature

AMSL
Above Mean Seal Level
BNB
Blue Nile Basin
CHIRPS
Climate Hazards Group InfraRed Precipitation with Station data
 CV_{nat}
Coefficient of Variation of the monthly natural flow
 CV_{reg}
Coefficient of Variation of the monthly regulated flow
DDP
Deterministic Dynamic Programming
DEM
Digital Elevation Model
ET
Evapotranspiration
FSL
Full Supply Level
GERD
Grand Ethiopian Renaissance Dam
GLDAS
Global Land Data Assimilation System
GRanD
Global Reservoir and Dam
HAD
High Aswan Dam
HP
Hydropower Production
MALR

Ministry of Agriculture and Land Reclamation
MODIS
Moderate Resolution Imaging Spectroradiometer
MWRI
Ministry of Water Resources and Irrigation
NRB
Nile River Basin
 R_{dam}
Reservoir Release
 R_{min}
Minimum Dam Release
 R_{max}
Maximum Dam Release
 $R_{turbine}$
Turbine Flow
RF
Regulation Factor
SEBAL
Surface Energy Balance Algorithm for Land
SRTM
Shuttle Radar Topography Mission
USBR
United States Bureau of Reclamation
VIC
Variable Infiltration Capacity
WaSSI
Water Supply Stress Index
 WC_{AG}
Irrigation Water Consumption
 WS_{SW}

* Corresponding author at: Department of Civil and Environmental Engineering, More 201, University of Washington, Seattle, WA 98195, United States.
E-mail address: fhossain@uw.edu (F. Hossain)

Surface Water Supply

1. Introduction

Many river basins world-wide are experiencing increasing pressure on water resources, due to accelerated economic growth, rising population, increasing food demand, and climate change (Wada and Bierkens, 2014; Munia et al., 2016). Such challenges are more evident in transboundary basins, e.g., the Nile basin (Paisley and Henshaw, 2013; Rahman, 2013), Euphrates-Tigris (Kibaroglu and Gürsoy, 2015), or the Mekong basin (Grumbine and Xu, 2011). These rivers are under intense development pressure, with multiple upstream dams planned or under construction that would dramatically alter a wide range of hydrological, agricultural, and ecological systems. In addition to dam development, climate variability is a significant factor when assessing water system sustainability (Vörösmarty et al., 2000; Kumm et al., 2014). The growing regional and global concerns about these adverse impacts of large-scale dam construction and climate variability have led to increasing interests to revisit the operation of existing dams (Grumbine et al., 2012; Digna et al., 2018).

Considering the growing number of dams under construction (more than 600 dams globally according to Zarfl et al., 2015), it is now timely to re-assess the impact of these emerging and upstream dams on downstream regions, particularly on existing reservoirs that are the mainstay of water security for those countries. The Nile River Basin (NRB) presents a classic and timely case for such a re-assessment with eleven transboundary countries that are continuously competing for scarce water resources to support a growing population and economic development challenges (Molden et al., 2009). For instance, Ethiopia and Sudan are now moving towards building new hydropower dams, which are expected to provide the primary source of electricity. Building such dams can significantly alter downstream water availability for Egypt, especially during the filling phase of the dam's reservoir. With irrigation and hydropower as key drivers of economic and social development in the NRB, any development by upstream countries would lead to considerable friction and tensions on the use of the water among the riparian nations.

The announcement of the construction of Grand Ethiopian Renaissance Dam (GERD) in 2011 and the disagreements that ensued between Egypt and Ethiopia exemplifies a transboundary water challenge. The GERD project challenges Egypt's historical hegemonic position on the Nile basin and aspires to project the power of Ethiopia on Nile water sharing (Whittington et al., 2014; Cascão and Nicol, 2016). As ongoing dam projects expand in the upstream portion of the NRB, water resources managers will need to advocate for the sustainable use of available water resources while ensuring the development goals for all countries. In the case of transboundary basins, employing adaptive management is currently best-suited to confront impending challenges and mitigate the impacts downstream of the basin (Pahl-Wostl, 2007; Zeitoun et al., 2013). Thus, it is crucial to adapt the operation of existing reservoirs in NRB, e.g., High Aswan Dam in Egypt, to upstream planned dams that are already under construction, e.g., GERD. An adaptive reservoir operation includes learning from the status quo downstream management practices to adapt better to future challenges (Georgakakos et al., 2012; Zhang et al., 2017).

The High Aswan Dam (HAD) forms the largest storage dam in the Nile basin (total storage capacity of 162 km³) and is considered as the faucet that controls the water flowing downstream in Egypt. HAD operation is based on the Nile Waters Agreement of 1959 between Egypt and Sudan (assuming an annual average inflow of 55.5 km³ allocated to Egypt) and under the assumption that most of the Blue Nile flow will contribute as unregulated inflow to HAD. The upper Blue Nile, i.e., upstream of the GERD location, provides about 53% of the annual flow

reaching downstream to Egypt. Therefore, introducing a large-scale dam like GERD into the Blue Nile will inevitably impact the flow reaching HAD during filling and later during operations of GERD. Such impacts, for example, include changes in the total annual flow volume reaching downstream (primarily during the GERD filling) and the seasonal timing of flow (primarily during the GERD post-filling phase). In addition, Egypt's water sustainability downstream, particularly for agricultural uses, is threatened as HAD currently lacks provision to adapt to GERD filling and operations. Therefore, it is important for a downstream country like Egypt with its growing population, to understand what changes GERD will bring to its water security and how HAD needs to adapt its operation to such imminent challenges.

Understanding impacts on reservoir operation is difficult in transboundary basins due to the historical lack of shared in-situ information on reservoir operation and water management practices (Hossain et al., 2007; Balthrop and Hossain, 2010). However, such information is now becoming available from satellite remote sensing. Satellite data can provide estimates of different components of hydrological cycle including precipitation, evaporation, water level, water area, and soil moisture, which can then be used to predict the state of a reservoir (Famiglietti et al., 2015; Lettenmaier et al., 2015; Sheffield et al., 2018). Recently, satellite measurements have been successfully incorporated in reservoir models to understand the operation of dams in transboundary basins (e.g., Bonnema and Hossain, 2017; Eldardiry and Hossain, 2019). For example, Eldardiry and Hossain (2019) have developed a satellite-based framework to derive the operating rules of HAD in the Nile basin. The centerpiece of this framework is the hydrological model that exploited the global availability of satellite observations at high spatial and temporal resolution as forcing inputs. Our study builds upon this tested satellite-based modeling framework (Eldardiry and Hossain, 2019) to address the following key question: *How can a downstream and pre-existing dam such as the HAD, adapt its operation to inflow alterations during the filling and operation phases of a newer dam in the upstream, such as the GERD?*

The adaptation of HAD operation to GERD construction typifies one of the challenges facing dam operators and water managers in downstream Nile riparian countries. Recently, various studies have investigated the impacts of GERD on downstream countries with more focus on the GERD filling strategies (King and Block, 2014; Mulat and Moges, 2014; Zhang et al., 2015; Wheeler et al., 2016). However, crucial insights on how dam operators can adapt to potential impacts have not been capitalized in previous studies. For example, Zhang et al. (2015) concluded reduction in downstream streamflow due to various factors including filling policy of GERD, climate variability, and projected climate change scenario. Wheeler et al. (2016) and Wheeler et al. (2018) introduced some HAD operation scenarios, drought (or no drought) management policy, based on GERD agreed annual release (cooperative approach). However, Wheeler et al. (2016) and Wheeler et al. (2018) focused only on the total annual shortages in HAD inflow without insights into the potential changes in HAD operation based on downstream agricultural adaptations. Our study proposes a physical blueprint that employs water scarcity indices to infer modified reservoir operation to adapt to expected streamflow alterations while maintaining the supply for downstream water use. Reinventing the operating curves for existing dams will provide an inclusive understanding of the potential adaptation alternatives to future challenges associated with planned dams and streamflow variability. The remainder of the paper is organized as follows. We describe the study area and the selected dams in Section 2, data sources and methods are introduced in Section 3, results for the HAD reservoir operation under GERD filling and operation scenarios are discussed in Section 4, discussion of results and concluding remarks are summarized in Sections 5 and 6, respectively.

2. Study area and dams

The Nile River Basin (NRB) is a major transboundary river that passes through eleven countries in northeastern Africa (Fig. 1). The NRB comprises two major tributaries, the Blue Nile (originates from the Ethiopian plateau) and the White Nile (originates from Lake Victoria in Jinja, Uganda). The Blue Nile is the primary tributary of the main Nile River, providing about 62% of the flow reaching Aswan (Mellesse et al., 2011). The NRB is currently undergoing hydropolitical changes through the construction of large scale dams and the expansion of irrigation projects (Aljefri et al., 2019). Fig. 1 shows the existing, planned, and under construction dams along the Nile river according to the Global Reservoir and Dam (GRand) database (Lehner et al., 2011), the Global geOreferenced Database of Dams (GOODD) (Mulligan et al., 2020), and Zarfl et al. (2015). The purposes of the major dams in the NRB (e.g., High Aswan Dam in Egypt, Roseires and Merowe dams in Sudan, and Nalubaale Power Station in Uganda) are to produce hydroelectric power and provide water supply needed to meet irrigation demands. The future hydropower dams inventory produced by Zarfl et al. (2015) reveals an increasingly impounded Nile river for hydropower development in NRB with more than 35 dams planned for construction. The current study focuses on the impacts of the Grand Ethiopian Renaissance Dam (GERD), currently under construction on the Blue Nile, on the operation of the downstream High Aswan Dam (HAD) in Egypt. The area-elevation curve was established for the two reservoirs (i.e., lakes of HAD and GERD) using a 30 m resolution digital elevation model (DEM) provided by the Shuttle Radar and Topography Mission (SRTM) (for more details on deriving area-elevation curves of HAD and GERD using SRTM, the reader is referred to Eldardiry and Hossain (2019) and ElBastawesy (2014), respectively). The satellite-driven curves (both Area-Elevation and Volume-Elevation curves) were compared with those published in previous stud-

ies (Abteu and Dessu, 2019; Basheer et al., 2020 for GERD) and (Husrt et al., 1966; Moussa, 2018 for HAD). Our comparison shows robust skill to infer the reservoir volume at different elevations for GERD and HAD with a mean percentage error of 7% (compared to Basheer et al., 2020) and 9% (compared to Husrt et al., 1966), respectively. Thus, satellite-driven curves can be very useful in inferring reservoir characteristics, e.g., storage level and volume, especially in transboundary basins, where bathymetric surveys are usually not available (Bonema and Hossain, 2017, 2020). The specifications of the HAD and GERD are summarized in Table 1 and explained as follows.

2.1. High Aswan dam (HAD)

The High Aswan Dam (HAD) is an embankment dam built across the Main Nile in Aswan, Egypt between 1960 and 1970 to provide long-term protection against drought and flood (Abd-El Monsef et al., 2015). HAD regulates the inflow primarily to meet the downstream water supply for irrigation demands in Nile Delta and along the Nile Valley (Fig. 1), where 96% of Egypt's population is located. The HAD also serves hydropower generation, and water supply for industries and municipalities. The HAD reservoir, Lake Nasser, started impounding in 1964 and reached an operating level (175 m above mean sea level-AMSL) in 1975 (El-Shabrawy, 2009; Moussa, 2018). The operation rules of Lake Nasser reservoir are designed to ensure adequate water supply and safety of the HAD. The HAD reservoir has a total storage of 162 km³ with minimum and maximum operating levels of 147 m and 182 m AMSL, respectively. At the beginning of the water year (1st of August), the water level is kept at 175 m AMSL (Full Supply Level) to store incoming high flows (Moussa, 2018). The storage increases gradually in the summer and, subsequently, the reservoir levels decrease from January to July as water is released. The HAD is equipped with six pairs of turbines, each having a capacity of 175 MW,

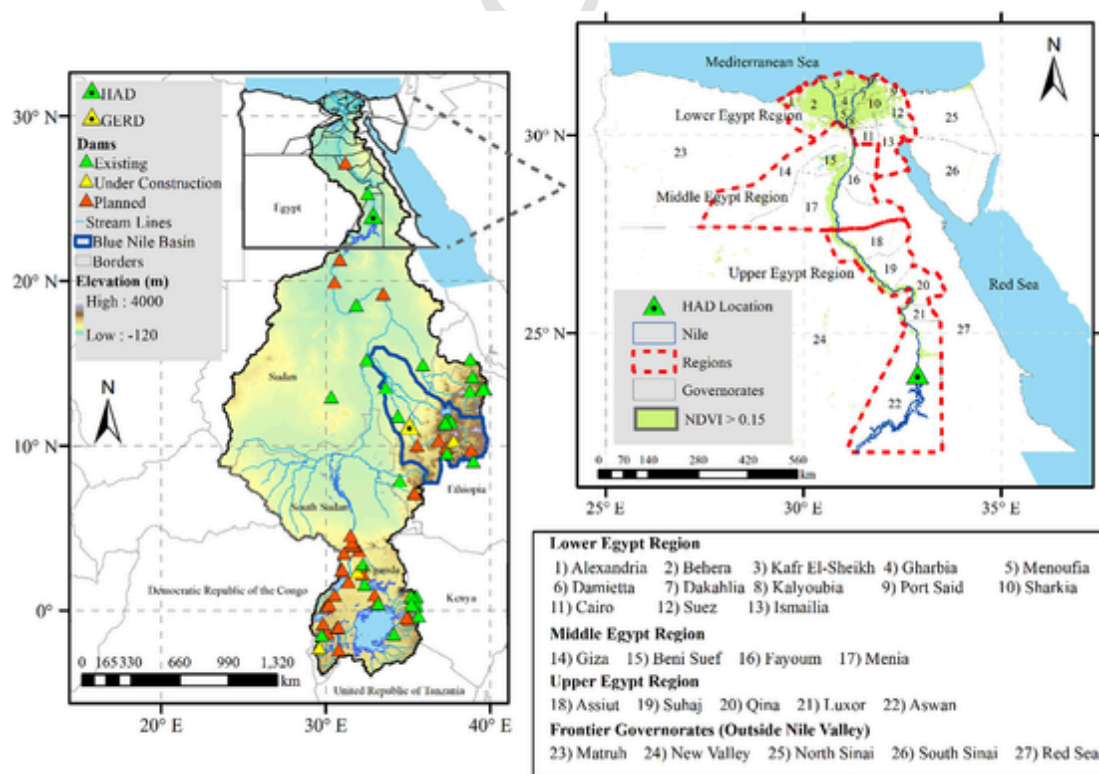


Fig. 1. The Nile River basin (NRB) with the existing, planned, and under construction dams as provided by the GRand database (Lehner et al., 2011), GOODD database (Mulligan et al., 2020), and Zarfl et al. (2015). The right panel highlights the location of the HAD dam and the downstream agricultural area in the Nile Delta and along the Nile valley.

Table 1
The specifications of the existing downstream dam (HAD) and planned upstream dam (GERD).

Specification	HAD	GERD
Ground and Crest Levels	85–196 m	500–655 m
Minimum Operating Level	147 m	590 m
Full Supply Level (AMSL)	175 m	640 m
Emergency Spillway Level	178 m (Toshka spillway)	642 m
Storage (km ³)	162 km ³ (Dead = 32 km ³ – Live = 90 km ³ – Emergency = 40 km ³)	74 km ³ (Dead = 14.8 km ³ and Live = 59.2 km ³)
Hydropower Capacity (Turbines)	2100 MW (12 Turbines)	5150 MW (16 Turbines)

and the power station has total capacity of 2100 MW (Table 1). One pair of turbines is assumed inoperative at any time because of maintenance problems, and another turbine is left idle to provide spinning reserve (Thomas and Revelle, 1966; Moussa et al., 2018). The maximum annual hydropower production at the dam is therefore considered to be 1134 GWH per month (assuming the full operation of 9 turbines during the month). In our study, we assumed a more conservative approach to the estimation of hydropower production capacity by applying a 50% load factor to the maximum production, yielding a value of 567 GWH/month (or 6804 GWH/year).

2.2. Grand Ethiopian Renaissance dam (GERD)

The Grand Ethiopian Renaissance Dam (GERD) location was first identified in a study conducted by the US Bureau of Reclamation to explore the potential hydropower dam sites in the Blue Nile Basin (USBR 1964). The construction site of the main dam is at a ground level of 500 m above mean sea level (AMSL) and can only store water with a maximum level of 606 m AMSL (ElBastawesy, 2014). The current design of GERD is to supply a storage at an elevation of 640 m (Full Supply Level) with a corresponding capacity of 74 km³. The main dam is supported by a rock-fill saddle dam (to the west of the GERD) to provide the storage between 606 m and 640 m (Abteu and Dessu, 2019). The GERD is planned to have 16 turbines with a total capacity of 5150 MW, making it the largest hydropower dam in Africa and it is likely to bring significant improvements to the electricity access for the entire Nile (MIT 2014).

3. Methods and data

This study presents an integration of models with satellite observations to re-evaluate the operation of HAD (the pre-existing downstream dam) under the impacts of GERD (the upstream dam currently under construction). Revisiting the operation of the HAD during the filling and operation phases of GERD followed a modeling blueprint that integrates satellite observations into hydrological and reservoir modeling as illustrated in Fig. 2. The adaptation of HAD operation to GERD filling/operation phases is then assessed by building different scenarios of HAD operation under the impacts of different factors including: GERD filling period, initial storage level at HAD, and the downstream supply stress levels (Table 2). The proposed blueprint comprises four main components that are described in the next sections.

3.1. Reservoir inflow scenarios

To understand the filling and operation scenarios of a planned dam, hydrologic information on the watershed upstream of the dam is required. Such information includes precipitation, lake evaporation, and reservoir inflow. In our study, we used the Variable Infiltration Capacity (VIC) model to simulate the hydrologic conditions over the upper Blue Nile Basin (BNB). The VIC model was implemented at 0.1° (~10 km) spatial resolution for the BNB and driven by high spatial and temporal resolution of satellite observations, e.g., SRTM, CHIRPS, and MODIS. The previous study by Eldardiry and Hossain (2019) has demonstrated the fidelity of the VIC model with satellite observations for simulating streamflow along the BNB (validated at Khartoum and Eldiem stations with a Nash Sutcliffe Efficiency of 0.68 and 0.92, respectively). For further details, the reader is referred to Eldardiry and Hossain (2019) for understanding the VIC modeling framework over the BNB. The satellite-driven VIC model for the BNB is used in this study to characterize the streamflow climatology upstream of the GERD (inflow at Eldiem station) for 37 years (1981–2017). The use of 37-year streamflow climatology allowed the assessment of GERD filling/operation scenarios under expected inter-annual and intra-annual variability of streamflow. Such variability is significant in the annual Nile river flows (Siam and Eltahir, 2017) and is expected to increase in future with climate change (Conway, 2017).

In our study, we followed a GERD filling approach that assumes monthly filling of the dam in a pattern identical to its inflow, i.e., higher storage in summer months, during a number of filling years that satisfies the total dam storage capacity (74 km³). In each filling year, we assumed the volume stored in the reservoir is proportional to the

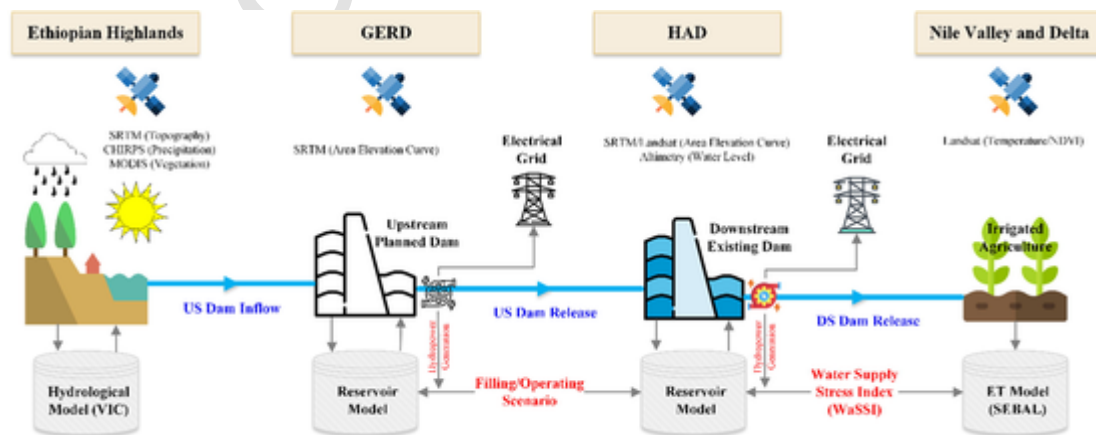


Fig. 2. Schematic diagram of the blueprint proposed in our study to re-evaluate the operation of existing dam under the filling/operation of an upstream planned dam.

Table 2

Decision factors considered in the assessment of HAD operation under the filling/operation of GERD (upstream dam).

Decision Factor	Scenario
Upstream dam (GERD)	Filling vs operation phase
GERD filling period	2 to 12 years
HAD and GERD inflow	Dry vs normal vs wet years
HAD initial storage level	Low vs high
Downstream stress level	Status quo stress vs predefined stress level

total dam inflow. Thus, the storage volume (S_i) for each year of filling is calculated as follows:

$$S_i = S_{\max} * \frac{Q_i}{\sum_{i=1}^N Q_i} \quad (1)$$

Where Q_i is the total annual flow volume (in km^3) for year (i) of filling, N is the total number of filling years, S_{\max} is the storage capacity of the dam (74 km^3 for GERD). We used the historical inflow (1981–2017) simulated by the VIC model at Eldiem station to calculate the possible range of GERD releases assuming different scenarios of GERD filling (ranging from 2- to 12-year filling scenarios). To account for the streamflow variability and possible filling years with dry or wet hydrologic conditions, we filled the dam during a moving time window of N years for each N -year filling scenario. For example, for a 3-year filling scenario, we produced 35 possible climatological conditions to fill the dam in 3 years (the first window is between 1981 and 1983 and the last window is between 2015 and 2017). Similarly, for a 12-year filling scenario, the first window includes the inflow for years between 1981 and 1992 and the last window assumes filling years between 2006 and 2017.

We assumed the filling of GERD will start in August, when the flow in the upper BNB is at its peak. The monthly inflow to the HAD reservoir was obtained by routing the GERD outflow in the BNB to Khartoum station and adding the monthly flow from the White Nile and Atbara River. To include the interannual variability in the flow from the White Nile and Atbara river, we considered three scenarios that reflect normal (average flow), dry (average - standard deviation), and wet (average + standard deviation) flow conditions (Fig. 3a). These conditions resulted in additional annual flow to the HAD that ranges from 26 km^3 (dry conditions in White Nile and Atbara river) to 48 km^3 (wet conditions in White Nile and Atbara river). When GERD starts filling, we assumed the initial level of the HAD to be at low (169.32 m AMSL) or high (178.37 m AMSL) storage conditions based on HAD operation in the recent years (2011–2020) (Fig. 3b). The HAD levels are estimated based on radar altimetry-based water surface elevations that

were acquired from the operational satellite altimetry Hydroweb database (Crétau et al., 2011).

3.2. Irrigation water use

Agriculture is the dominant water use in the eastern Nile countries. In Egypt, 86% of the HAD releases are consumed by the agricultural sector, while the remaining 14% are shared between municipalities and industrial sectors (FAO 2016). Hence, the expected changes in the HAD inflow, as a result of GERD filling and/or operation, will inevitably impact agricultural consumption downstream of HAD. Adapting the current operation of HAD to upstream changes requires a thorough understanding of the crop patterns in Egypt and subsequently the water requirements for irrigation. A common approach to represent the irrigation demand by a specific crop is to use the evapotranspiration as a proxy of the water consumptive use. Evapotranspiration (ET_c) is a key component of the hydrologic cycle and its accurate estimation is of vital importance for hydrologic water balance, irrigation system design and management, and water resources planning and management (Fisher et al. 2017).

To address ET_c variability in regions with limited ground-based measurements, as is the case in the NRB, satellite images are an excellent means for determining and mapping the spatial and temporal structure of ET_c (Allen et al., 2007). Various satellite-based methods have been suggested in literature (Liou and Kar, 2014), e.g., SEBAL (Surface Energy Balance Algorithm for Land) and METRIC (Mapping Evapotranspiration at High Resolution and with Internalized Calibration). Such remote sensing approaches can provide accurate and more frequent monitoring of the crop water requirements in regions where in-situ data are not readily available. In our study, we employed the Surface Energy Balance Algorithm for Land (SEBAL) algorithm (Bastiaanssen et al., 1998, 2005). SEBAL has been successfully implemented in previous studies to estimate ET using satellite images (e.g., Senay et al., 2016; Elnmer et al., 2019). In the SEBAL model, ET is computed from satellite images and weather data using the surface energy balance. SEBAL calculates ET through a series of computations that generate: net surface radiation, soil heat flux, and sensible heat flux to the air. A residual energy flux is then calculated by subtracting the soil heat flux and sensible heat flux from the net radiation at the surface. This residual energy is used to convert the liquid water into water vapor (or latent heat flux), i.e., evapotranspiration. Therefore, the ET flux is calculated for each pixel of the image as a residual of the surface energy budget equation:

$$\lambda ET = R_n - G - H \quad (2)$$

where; λET is the latent heat flux (W/m^2), R_n is the net radiation flux at the surface (W/m^2), G is the soil heat flux (W/m^2), and H is the sensible heat flux to the air (W/m^2).

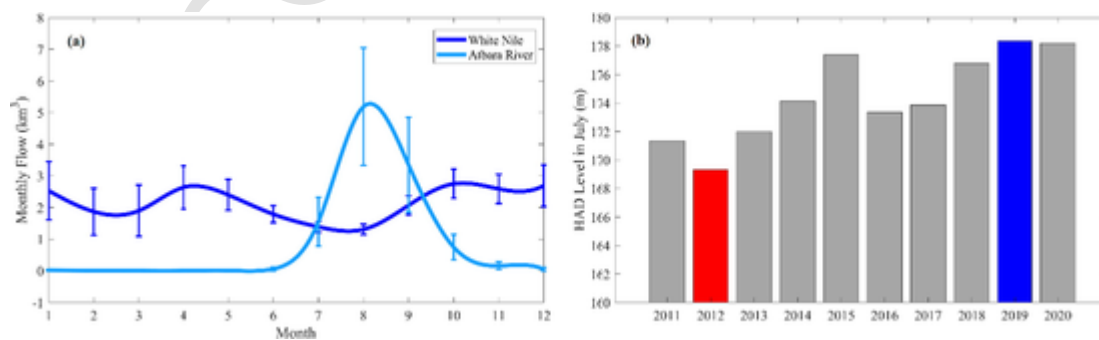


Fig. 3. a) The average monthly flow at the outlet of White Nile and Atbara rivers (error bars indicate the standard deviation) [Data Source: Global Runoff Data Centre (GRDC)]. b) The HAD level in July in the recent years (2011–2020). The red and blue bars indicate the lowest and highest water level that are used in our scenario assessment as initial storage HAD level when GERD starts filling [Data Source: Hydroweb database]. (For interpretation of the references to colour in this figure legend, the reader is referred to the web version of this article.)

In our study, the SEBAL was applied on freely available Landsat-8 satellite images to estimate total ET_c over different governorates (administrative boundaries in Egypt) located downstream of the HAD reservoir (see Fig. 1). The monthly SEBAL-based ET_c was estimated for the period between January 2014 and December 2017 (the most recent years of our VIC simulations). The SEBAL model also requires the meteorological data of land surface, such as wind speed, surface pressure, and air temperature as inputs for the surface energy balance calculations. The meteorological data of land surface were obtained from the outputs of the Global Land Data Assimilation System (GLDAS) (Rodell et al. 2004). GLDAS outputs have been evaluated globally with high accuracy in northern Africa when compared with gauge-based counterparts (see for example Decker et al. (2012) and Ji et al. (2015)). To avoid the misclassification of non-vegetation areas, we modified the SEBAL algorithm by adding random forest classification scheme to mask all areas that are not considered as potential agricultural area. The SEBAL parameters, e.g., hot and cold pixel selection, are calibrated using the irrigation water use data retrieved from the annual bulletin of water resources and irrigation, issued by the Central Agency for Public Mobilization and Statistics (CAPMAS) in Egypt, which is provided for each governorate downstream of the HAD (CAPMAS, 2014).

3.3. Water scarcity index

To understand water stresses downstream of the HAD, we adopted the water supply stress index (WaSSI) approach (Falkenmark, 1989; Sun et al., 2008; Eldardiry et al., 2016; Borrok et al., 2018). The WaSSI index is expressed as a ratio of water demand to water supply. Thus, the higher the WaSSI value, the more stress the water system faces. In our GERD/HAD assessment, we include two sectoral-based WaSSI indices to address the stresses due to agricultural water use and hydropower generation as follows:

$$WaSSI_{AG} = \frac{WC_{AG}}{WS_{SW}} = \frac{ET_c}{R_{dam}} \quad (3)$$

$$WaSSI_{HP} = \frac{R_{turbine}HP}{R_{dam}} \quad (4)$$

Here WC_{AG} is the irrigation water consumption calculated using the SEBAL model (ET_c) as explained in the (3.2), WS_{SW} is the surface water supply which is set equal to the total reservoir release (R_{dam}) (i.e., summation of both turbine and spillway discharges, while accounting for downstream environmental flow). $R_{turbine}$ is the turbine flow required for hydropower production (HP) based on downstream electricity demand. $R_{turbine}$ (in m^3/sec) is calculated using the following equation:

$$R_{turbine} = \frac{HP}{\eta\gamma h} \quad (5)$$

where HP is the hydropower production (watt), η is the power plant efficiency, γ (N/m^3) is the specific weight of water, and h (m) is the effective head of water (m) calculated as the height between open water surface elevation and turbine elevation.

3.4. WaSSI-Based optimal reservoir operation

To infer an optimal operating policy of the reservoirs under study (GERD and HAD), a deterministic dynamic programming (DDP) approach is followed. The DDP approach was originally developed by Karamouz and Houck (1982) and modified here to optimize the dam operation using the WaSSI index. A penalty function is first assumed to decide the range of acceptable dam releases (or the safe zone). Beyond this range, an increase in release may result in flooding downstream of the dam, while reduction in release will cause drought conditions with water shortage for downstream demands (Fig. 4). Similar to Kara-

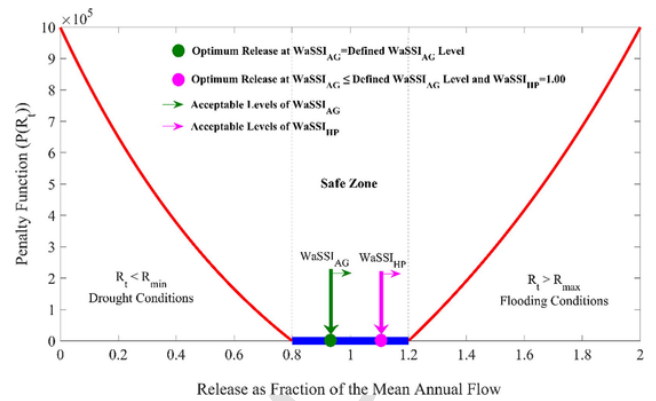


Fig. 4. Illustration of the Discrete Dynamic Programming (DDP) method based on the WaSSI stress index.

mouz and Houck (1982), a piecewise exponential form of the penalty function $P(R_t)$ is used as follows:

$$P(R_t) = \begin{cases} A \left[\exp\left(\frac{R_t}{R_{max}}\right) - \exp(1) \right] & R_t \geq R_{max} \\ 0 & R_{min} \leq R_t \leq R_{max} \\ B \left[\exp\left(-\frac{R_t}{R_{min}}\right) - \exp(-1) \right] & R_t \leq R_{min} \end{cases} \quad (6)$$

where R_t is the dam release at a time step (t), R_{max} is the maximum dam release or the upper limit of the safe zone, and R_{min} , is the minimum dam release or the lower limit of the safe zone. A and B are two constants that are defined based on how much damage will occur downstream the dam when the release is outside the safe zone. We here applied the same values used by Karamouz and Houck (1982) ($A = 3.88 \times 10^5$ and $B = 1.58 \times 10^6$) such that the penalty function would result in losses equal to 10^6 units when the release is zero or twice the mean annual flow (when assuming R_{max} is 120% of the mean annual flow). Applying DDP optimization approach, we used a set of discrete finite horizon of water levels with 0.01 m increments to derive monthly dam releases and the corresponding losses (from equation (6)). The safe range of water levels is defined as the zone with any release within the minimum and maximum dam release, i.e., zero penalty function (Fig. 4). The minimum and maximum HAD releases are set to 1.8 and 8.1 $km^3/month$, respectively based on the historical dam operation (Moussa et al. 2018). The optimal reservoir operation is then derived such that the total losses over a time horizon ($T = 37$ years of simulation) are minimized within the safe zone. An additional constraint is also added to find the release inside the safe zone that would ensure same or less than a defined WaSSI level. Fig. 4 shows a schematic of the penalty function integrated with the WaSSI stress to find the optimal reservoir release. The agriculture-based stress ($WaSSI_{AG}$) is prioritized in our optimization since the hydropower can be a by-product of the dam release for irrigation (i.e., $WaSSI_{HP} \leq 1$). In case when the dam release is not enough to produce the target hydropower (i.e., $WaSSI_{HP} > 1$), the DDP method keeps searching for release in the safe zone that would fulfill the hydropower demand (which in turn reduces the downstream $WaSSI_{AG}$).

4. Results

4.1. Status quo stresses downstream of HAD

Understanding the status quo stresses on the water system downstream of HAD is a key step to further explore the impacts of upstream dams on HAD operation. Since agriculture represents 86% of the water use downstream HAD, we focused our stress analysis on consumptive water use for irrigation. The irrigation water use in Egypt varies during three crop seasons: 1) the winter season starts from October to Decem-

ber and ends between April and June (main crops are wheat, clover, barley); 2) the summer crops from March to June and harvested from August to November (main crops are cotton, rice, maize, and sorghum); and 3) Nili season which is a delayed summer season between July and August (main crops are rice, and sorghum). High density of cropped areas are located in the Nile Delta in northern Egypt, where most of the water intensive crops are grown (e.g., rice and wheat). The percentage of cropped area in the Nile delta ranges between 62% in the winter to 65% in the summer to 46% in the Nili season (Table S1 in Supplementary material). Only 5% of the cropped area in Egypt are outside the Nile valley in the frontier governorates, which are mainly irrigated by groundwater from the Nubian Sandstone Aquifer System, e.g., Matruh and New valley or rainfall, e.g., Sinai.

The characterization of the cropping pattern downstream of the HAD is crucial to understanding the seasonal and spatial variations in crop water requirements. Fig. 5a shows the monthly evapotranspiration, as estimated by SEBAL, downstream of the HAD (calculated as the summation of ET_c over the governorates in upper, middle, and lower Egypt). The total annual water use of irrigation in Egypt ranges between 36.5 km^3 in 2015 and 43.4 km^3 in 2014 (average ET_c over the 4 years $2014\text{--}2017 = 40.3 \text{ km}^3$). The ET_c in Egypt features a bimodal pattern with two peaks in March and August with an average of 4.2 km^3 and 4.5 km^3 , respectively. In terms of spatial variations (figure not shown), the Nile Delta (lower Egypt region) has the highest annual water use, due to the growing of highly water intensive crops, e.g., wheat in winter and rice in summer (Table 1). For example, the annual water consumption by irrigation in Behera governorate is 5.4 km^3 which constitutes about 13.5% of the total irrigation water in Egypt.

The HAD releases for the recent years (2014–2017) are derived based on the satellite-based framework developed by Eldardiry and Hossain (2019) to monitor the HAD operation (Fig. 5b). The operation of HAD for irrigation purposes is determined based on seasonal plan (prepared by the MALR) of downstream irrigation requirements (Gouda, 2016). Most of the water released from HAD are directed downstream to Nile Delta where most of the cropped lands are located (with an average total annual release of 65 km^3). Combining the information on water use (from SEBAL ET_c) and water supply (from HAD releases), we calculated the annual and monthly stress index ($WaSSI_{AG}$) downstream of the HAD. The annual stresses indicate stress levels less than one (i.e., HAD releases are sufficient to meet downstream agricultural demands), with an average stress of 0.63 (the highest $WaSSI_{AG} = 0.76$ in 2014). Looking closer at monthly scale (Fig. 5c) portrays a better understanding of the seasonal variations in the stress. While the stresses are exacerbated in the winter months with average stresses exceeding one in February (average $WaSSI_{AG} = 1.32$), lower stress levels are noticed in the summer months (e.g., average $WaSSI_{AG} = 0.40$ in June). The seasonal discrepancy in the monthly stresses is attributed to the low (or high) flows released in the winter (or summer) months (Fig. 5b). During the winter months, insufficient supply of HAD releases is encountered by relying on rainfall, as the

case in northern regions (e.g., Alexandria, Behera, and Kafr El-Sheikh governorates), or by pumping groundwater. In addition, the stress variation across months highlights the opportunities to derive better operating rules for HAD by managing the downstream stresses, especially in years when inflow is expected to be reduced by GERD filling.

4.2. HAD under filling scenarios of GERD

The GERD reservoir is considered completely filled when the reservoir storage reaches its maximum capacity of 74 km^3 . Not surprisingly, as the number of filling years increases, the GERD release becomes less sensitive to the filling duration (Fig. 6). For instance, the difference in the median GERD release between the 7- and 6- year filling scenario is 1.5 km^3 compared to 6.5 km^3 difference between the 3- and 4- year filling scenarios. The results agree to great extent with Wheeler et al. (2016) who followed a more cooperative scenario that assumes an agreed annual release for filling the GERD. For example, if the downstream countries agreed to an annual release of 35 km^3 , Wheeler et al. (2016) found that it would take an average of 6 years to fill the dam. Similar results can be inferred from Fig. 6 for a 6-year scenario that corresponds to a median GERD release of 35.32 km^3 . The annual assessment of GERD filling indicates that downstream flow can be highly affected by short filling periods with more than 30% of reduction in Blue Nile inflow with filling scenarios of less than six years. With longer periods of filling (>6 years), smaller differences are noticed between the GERD release and thus lesser impacts on downstream flow.

The GERD releases during the filling scenarios are routed downstream to Khartoum station and then added to the flow from the White Nile and Atbara river to form the total inflow into HAD. Fig. 7 shows the changes in HAD water level when considering the 3- and 7-year GERD filling scenarios, which represent two examples of fast- and slow-paced filling proposals, respectively. The HAD water level is calculated under two different scenarios of downstream $WaSSI_{AG}$ stress level; first, we consider the status-quo conditions that resulted from our analysis in Section 4.1. Second, we assumed a predefined constant $WaSSI_{AG}$ levels throughout the year (only $WaSSI_{AG} = 0.70$ is shown in Fig. 7). The predefined $WaSSI_{AG}$ level represent an adaptation scenario by HAD operators to the impacts of GERD filling. For example, the stress level of 0.70 will result in lower stresses in the winter months, which means either less cropping areas or finding alternative resources like groundwater or precipitation. Conversely, the stress will be elevated in the summer season (e.g., $WaSSI_{AG}$ in June will change from 0.40 to 0.70), which means storing more water in the HAD reservoir. The irrigation demand downstream of HAD is assumed the same during the filling period using the monthly average of SEBAL ET estimates shown in Fig. 5a. The changes in HAD operation under different scenarios are explained using the slope of a linear regression fitting to the water level signals during the filling period.

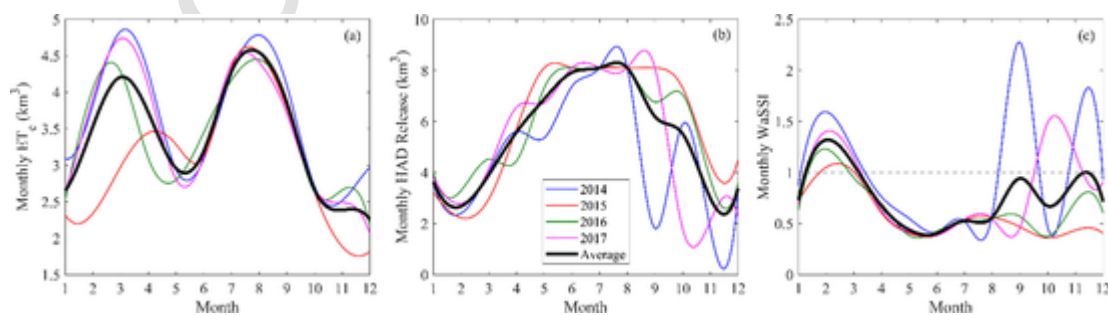


Fig. 5. Satellite-based estimates of the monthly evapotranspiration (SEBAL), HAD releases (Eldardiry and Hossain, 2019), and water stress index $WaSSI$ downstream of the HAD dam for the most recent years of the simulation period (2014–2017).

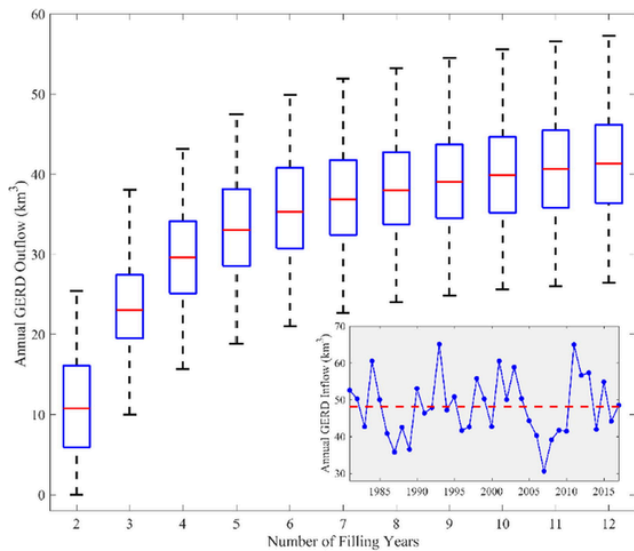


Fig. 6. The annual GERD outflow during different scenarios of GERD filling (2- through 12- year filling scenarios). The inset shows the historical (1981–2017) annual GERD inflow, i.e., naturalized flow (the red dashed line indicates the median streamflow). (For interpretation of the references to colour in this figure legend, the reader is referred to the web version of this article.)

Fig. 7 shows a significant drop in the HAD level when assuming a 3-year filling scenario, with more reduction in HAD storage if Egypt adopts the current stresses downstream of HAD (compared to a predefined $WaSSI_{AG} = 0.70$). A linear decreasing trend of (-0.30 m/month) is noticed in HAD level when employing the current $WaSSI_{AG}$ levels and assuming a scenario of low starting level at HAD reservoir. This trend can be alleviated by about 33% (slope = -0.20) if considering HAD will release less water to maintain a constant $WaSSI_{AG}$ level of 0.70. Similarly, a smaller decreasing trend (-0.14) is noticed when elevating the stress level to 0.70 for only months with $WaSSI_{AG} < 0.6$ (May through August), while keeping the other months at the current levels (figure not shown).

A flatter pattern is noticed for 7-year filling scenario with negligible trends (trend slope = -0.03 and 0.02 for current stresses and $WaSSI_{AG} = 0.70$, respectively). Fig. (7) also shows how HAD can operate if GERD filling starts when HAD is at high storage conditions, i.e., above the normal operation level (175 m), as the case noticed recently in July 2018 (HAD level is at 176.77 m) and 2019 (HAD level is at 178.37 m). While the trend slope is still negative when assuming high

initial HAD level scenario, the impacts on HAD operation are reduced with relatively high storage levels during GERD filling years. The HAD level at the end of the GERD filling period can be elevated by considering higher downstream stresses and/or longer GERD filling period (e.g., HAD level will reach 173.76 m with $WaSSI_{AG} = 0.70$ and 7-year filling period). Table 3 summarizes the scenarios in Fig. 7 and the corresponding changes in the trend slope and HAD level (at the end of the filling period).

The improvement in the HAD storage levels when adapting its downstream stress is primarily attributed to the increase in the stress level during the rainy season in the BNB (June to September). While the current HAD operation indicates higher releases during this rainy season, coping with future challenges requires revisiting the operating curve. For instance, our stress-based analysis suggests elevating the stress during the summer months, i.e., store more and release less. This approach will secure enough water during the low flow months while preserving the power generation production of the dam. The effect of streamflow variability is indicated with the standard deviation bars in Fig. 7. The higher variability was noticed in later years due to the use of a fixed initial HAD water level, i.e., 169.32 (178.37 m) for low (high) storage conditions, which resulted in narrower HAD storage options in the safe zone of DDP optimization (Fig. 4). As the filling progresses, the safe zone of optimization becomes wider and therefore the HAD level becomes more sensitive to inflow variability.

The combined effects of the GERD filling scenarios, HAD initial storage level, and downstream $WaSSI_{AG}$ stress condition on HAD operation is summarized by plotting the average HAD level at the end of the filling period under different stress conditions vs years of GERD filling (Fig. S3 in Supplementary material). The current average HAD level in July (174.47 m; averaged for the 10 years 2011–2020) can be reached when setting downstream stress level to 0.80 and assuming GERD to be filled in more than 8 years. When considering GERD filling scenario with high initial HAD level and $WaSSI_{AG}$ of 0.80, the HAD can reach its target operating level if GERD follows a filling scenario of more than 5 years. To further explain the impacts of streamflow variability (i.e., dry and wet years) on the HAD level, Figure (8) shows the cumulative probability of the HAD level at the end of the 3- and 7-year filling scenarios. Lower HAD levels are noticed under the current $WaSSI_{AG}$ levels or when setting $WaSSI_{AG} = 0.70$ with the chance of reaching the minimum operating level of 147 m. For example, the HAD level has a probability of 1% to reach 147 m in case of 3-year GERD filling scenario and applying the current stress levels downstream of HAD (Fig. 8a). Below this elevation (147 m AMSL) is the HAD dead

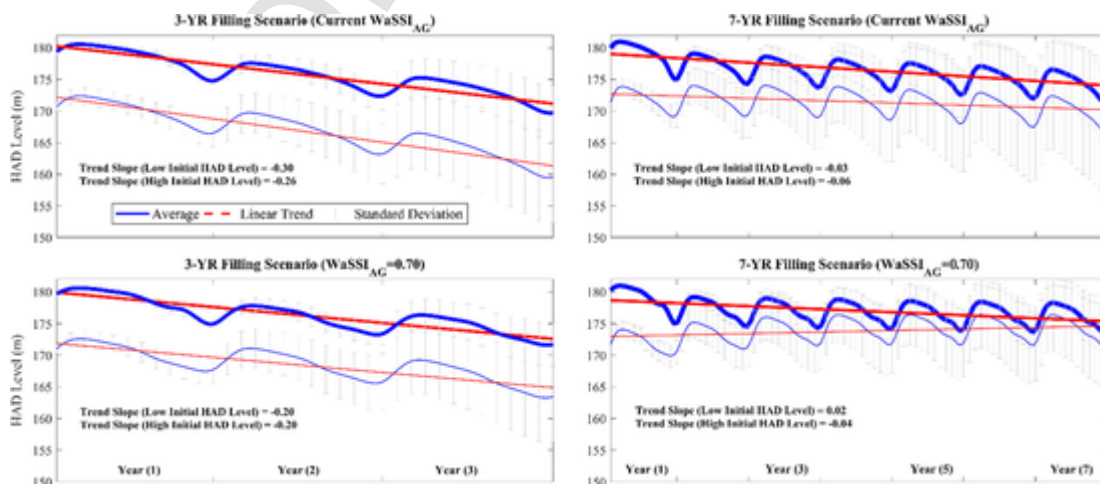


Fig. 7. The HAD water level (m) under the 3- and 7- year GERD filling scenarios with different levels of stress index $WaSSI$ (current stress levels vs predefined stress level = 0.70). The thick and thin lines indicate the scenarios with high and low initial HAD storage levels, respectively.

Table 3
Summary of the trend slope and HAD level (at the end of filling period) under different scenarios of GERD filling, initial HAD storage level, and downstream stress condition.

GERD Filling	Downstream Stress Conditions	Initial HAD Storage Level	Trend Slope	HAD Level* (m)
3-Year Filling Scenario	Non-Adaptive Approach (Current WaSSI _{AG})	Low	-0.30	159.52 (± 7.23)
		High	-0.26	169.73 (± 4.31)
	Adaptive Approach (WaSSI _{AG} = 0.70)	Low	-0.20	163.47 (± 7.15)
		High	-0.20	171.73 (± 3.42)
7-Year Filling Scenario	Non-Adaptive Approach (Current WaSSI _{AG})	Low	-0.03	167.13 (± 9.36)
		High	-0.06	171.57 (± 5.51)
	Adaptive Approach (WaSSI _{AG} = 0.70)	Low	0.02	171.75 (± 6.22)
		High	-0.04	173.76 (± 2.90)

* Average (± standard deviation) HAD level at the end of GERD filling period.

storage and therefore, HAD cannot operate to meet downstream water demand. Wheeler et al. (2016) concluded a similar probability range (1–2%) when drought management policy was implemented at HAD. Assuming a low initial HAD storage when GERD starts filling, the me-

dian HAD level varies across the different scenarios from 168.14 m (for 3-year filling and current stress levels) to 174.72 m (for 7-year filling and WaSSI_{AG} = 0.70). A more optimistic picture of the HAD levels can be demonstrated by the maximum HAD levels that can go up to more than 175 m AMSL (HAD normal operating level) when assuming a high initial storage HAD levels at different filling scenarios (Fig. 8b). The range of HAD levels shows the importance of considering the streamflow variability when assessing the operation of HAD during the filling of upstream dams.

It is important to adapt HAD operation to expected reduction in inflow (during GERD filling). The approach we followed in our paper is to tweak the downstream stress so that the water system becomes more stressed during the summer months instead of the status quo low stress conditions. As the stress is elevated, HAD has to be operated in a way that stores more water compared to current conditions (Fig. 9a). For example, in a 3-year GERD filling scenario, a stress level of 0.70 will store 7.9 km³ in August (release = 6.5 km³) compared to 6.4 km³ (release = 8.08 km³) when adopting the current stress levels. Despite assuming the same downstream WaSSI_{AG}, differences in the HAD releases between 3-year and 7-year filling is due to the effect of hydropower optimization (WaSSI_{HP}). As a result, the release is more controlled by hydropower production in some months (e.g., October through January) and therefore lower HAD levels will require releasing more water in case of 3-year filling. Similarly for a 7-year filling scenario, as HAD level is higher (compared to 3-year filling), less water will be released to attain the same hydropower stress WaSSI_{HP}.

GERD Operation (Post-filling Phase)

The operating rule for the GERD dam is not published and it is under a high level of negotiations between the three countries: Egypt, Sudan, and Ethiopia. A non-cooperative operation scenario (from the Ethiopian perspective) would only consider the optimization of the reservoir operation to maximize hydropower generation (given the dam location at the Ethiopian-Sudanese border). Following the optimization

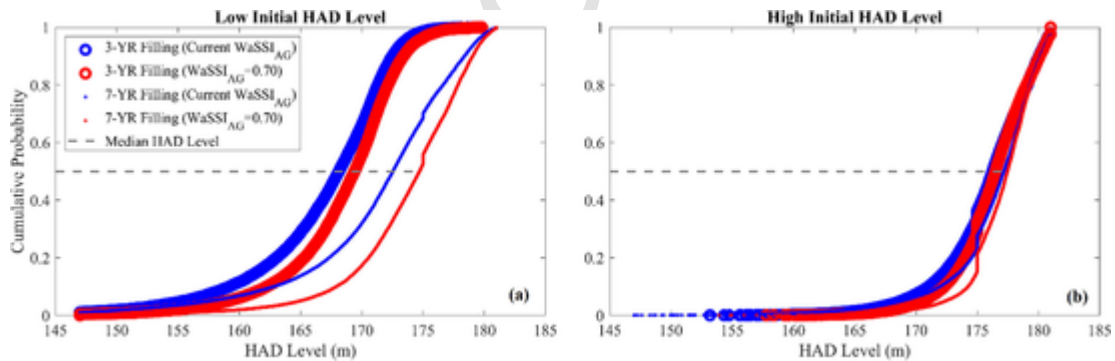


Fig. 8. The cumulative probability of HAD water level under different GERD filling scenarios and stress levels (WaSSI_{AG}) (pooling all monthly water levels during GERD filling scenario into one sample).

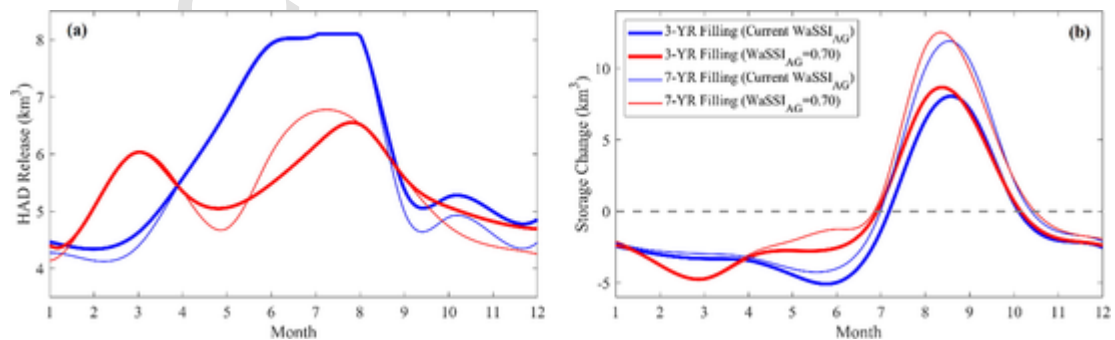


Fig. 9. HAD releases (a) and storage change (b) during the 3- and 7-year GERD filling scenarios (showing only the average of the hydrological sequences developed for each filling scenario and assuming an initial HAD storage at low level).

scheme explained in Section 3.4.2, GERD operation was derived to maximize hydropower generation. Additional constraints were added to the DDP problem by setting limits on storage capacity (or GERD levels), and minimum and maximum outflows, i.e., R_{\min} and R_{\max} in Eq. (6) (assumed to be equal to 0.80 and 1.20 of the mean annual inflow, respectively). Different hydrologic variables of the GERD reservoir operation are shown in Fig. 10. As expected, the derived GERD water levels are minimum in May before the rainy season (June through September) when the reservoir is being emptied (negative storage change in Fig. 9d) to be able to store the flow in the rainy season (Fig. 10a). The GERD reaches its maximum level in September (at the end of the rainy season) with an average equals to 636.96 m and standard deviation of 2.64 m. The average annual GERD outflow is about 48 km³ with the highest releases (5.56 km³) and storage change (9.17 km³) in September and August, respectively.

As indicated in Fig. 10a, the GERD will significantly regulate the downstream flow, with higher regulation during the non-rainy season, when the regulated flow is much higher than the naturalized flow. To quantify the regulation in the GERD outflow, we used a regulation factor (RF) to evaluate the change in the naturalized flow (GERD inflow) after GERD operation. The RF is calculated as follows (Zhou et al., 2018):

$$RF = \frac{CV_{nat}}{CV_{reg}} \quad (7)$$

Here CV_{nat} and CV_{reg} are the coefficients of variation (i.e., ratio of the standard deviation to the mean) of the monthly natural and regulated flow in the operation period, respectively. Three months (April, May, and September) have RF less than one (Table S2 in Supplementary material), which indicates that regulation by reservoir has limited impact on reducing the monthly variations in natural flow of the Blue Nile (downstream of GERD). The highest regulation of streamflow is noticed from November through February with regulation factor

ranges from 6.6 (in November) and 4.03 (in January), respectively. While the downstream flow is expected to reduce in the summer months (rainy season), the higher regulation in winter months balances such reduction by increasing GERD releases. These results agree with the percentage of GERD release estimated by Mulat and Moges (2014) who concluded that the minimum percentage released from GERD is within the wet months (July through October).

In terms of monthly streamflow variability, the months from June through November, which include mostly the rainy season in the BNB, experience reduction in monthly standard deviation with the largest decrease in August (69%) followed by October (58%). On the contrary, the months from December through May have significant increase in the monthly standard deviation of downstream flow (the largest increase is in January with percentage change of 338%). The high variability in the GERD release in September is attributed to the assumption of the dam being operated at Full Supply Level (FSL) of 640 m (e.g., Mulat and Moges, 2014; MIT, 2014; Wheeler et al., 2016). The FSL of 640 m does not yield enough storage capacity for the dam (i.e., 74 km³), especially during wet years when higher flows come in August and September. The GERD storage change peaks in August (average storage change = 9.17 km³); however, the dam fails to store enough of the inflow in September, and therefore, resulted in wider range of releases. This excess flow in wet years can also be released through the dam spillways, which would result in lower variations in September. The GERD operation was also tested for a higher FSL of 650 m (Fig. S5 in Supplementary material) and it yields a consistent variability throughout the year. For instance, the average monthly standard deviation dropped from 0.87 km³ to 0.73 km³ when changing the FSL from 640 to 650 m (compared to 1.14 km³ for the naturalized GERD inflow, i.e., without imposing the dam effect). The change in variability is affected by more regulation in the reservoir releases when assuming a FSL of 650 m. A higher FSL allows more outflows in the spring (months before the rainy season) and therefore the reservoir has a buffer to store more water in September. For example, the mean

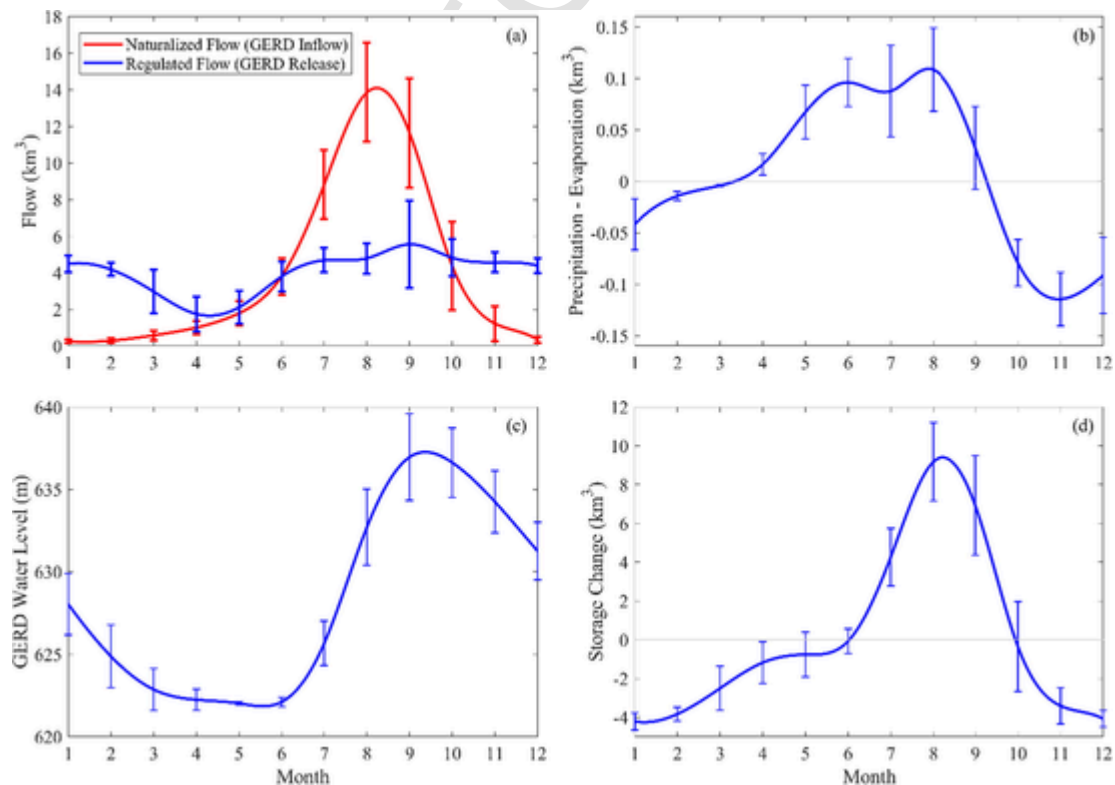


Fig. 10. Different hydrologic variables (inflow, precipitation-evaporation, water level, and storage change) during the GERD operation phase (FSL = 640 m AMSL).

GERD release in September changes from $5.56 \pm 2.39 \text{ km}^3/\text{month}$ (FSL = 640 m) to $4.74 \pm 0.75 \text{ km}^3/\text{month}$ (FSL = 650 m).

4.3. HAD during GERD operation

The HAD level at the end of the GERD filling period will drop down in most of the filling scenarios, e.g., the average HAD level at the end of the 3-year filling scenario is 159.52 m (169.72 m) when assuming low (high) HAD initial level scenario and adopting the current downstream stresses (Fig. 7). Thereby, there will be a recovery period for HAD to get back to its normal operation levels. Fig. 11 shows an illustrative example of how long it would take the HAD after the GERD filling to operate normally. Here, we considered HAD reaches its normal operation in the year when HAD level in September reaches at least 175 m (HAD normal operating level). In addition to the effect of HAD starting level, we accounted for streamflow variability and the possibility of the filling period to end in wet or dry years by considering: 1) the HAD level at the end of the GERD filling at normal, dry, and wet conditions (defined as average HAD level \pm Standard deviation) and 2) con-

sidering the GERD starting year of operation in different climatic conditions using a sliding window of one year in a 10-year period from 1981 through 1990 (these 10 years are selected as they include both wet (1984) and dry years (1986 to 1989)). Fig. 12 summarizes the range of HAD recovery years under different GERD filling scenarios and considering the impacts of streamflow variability on GERD/HAD operation. When applying the current levels of downstream stresses and after a 3-year filling scenario, the HAD will, on average, recover after 7 years (assuming a low initial storage level at HAD; Fig. 12a). If the water level at HAD is at a higher level (e.g., as the case of 2019 when HAD level reaches 178.37 m in July) when GERD starts filling (3-year filling scenario), the recovery period can be shortened significantly to only 3 years (Fig. 12c).

Similar to considering adaptation to downstream stress, recovery years also decrease when extending the filling period. For example, if considering a downstream $WaSSI_{AG}$ of 0.70 with a 7-year filling scenario, the recovery period can drop down to 2 years (compared to 3 years when assuming current stress levels downstream with a low initial level at HAD). Additionally, if HAD operators prepare in advance to GERD filling (scenarios of more than 9 years) by maintaining a high storage level and adapting the operation to a downstream stress level $WaSSI_{AG}$ of 0.70, HAD can operate normally immediately after filling the GERD without a recovery period (Fig. 12d). Furthermore, as indicated by the range of the boxplot, streamflow variability in the Nile tributaries (Blue Nile, White Nile, and Atbara) is a crucial factor to the HAD recovery period with longer ranges for short filling scenarios and low HAD initial level. For instance, in case of dry years, HAD can take more than 30 years (or 20 years if HAD is at high initial level) to recover from a 3-year filling scenario. The HAD recovery period highlights the connection between the GERD filling and the time HAD would take to refill its storage to a normal operation level. The results showed that the GERD filling period cannot offset the HAD recovery period, i.e., short filling will recover in a longer period but with similar overall time when compared to longer filling period with shorter recovery. This longer HAD recovery for the 3-year filling scenario arises from the larger storage volume (larger than GERD storage; 74 km^3) required

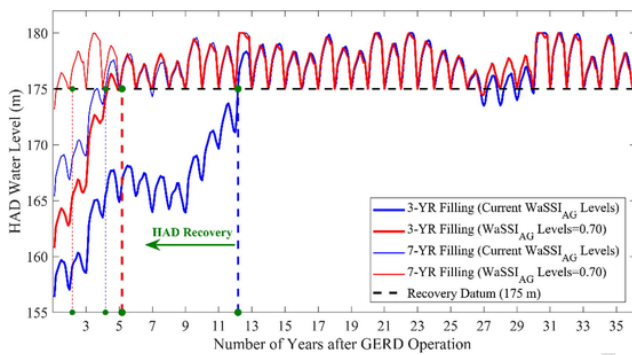


Fig. 11. Illustrative example of the HAD level recovery during the GERD operation after 3- and 7-year filling scenarios. The recovery period ends when HAD reaches its normal operation level (175) in September.

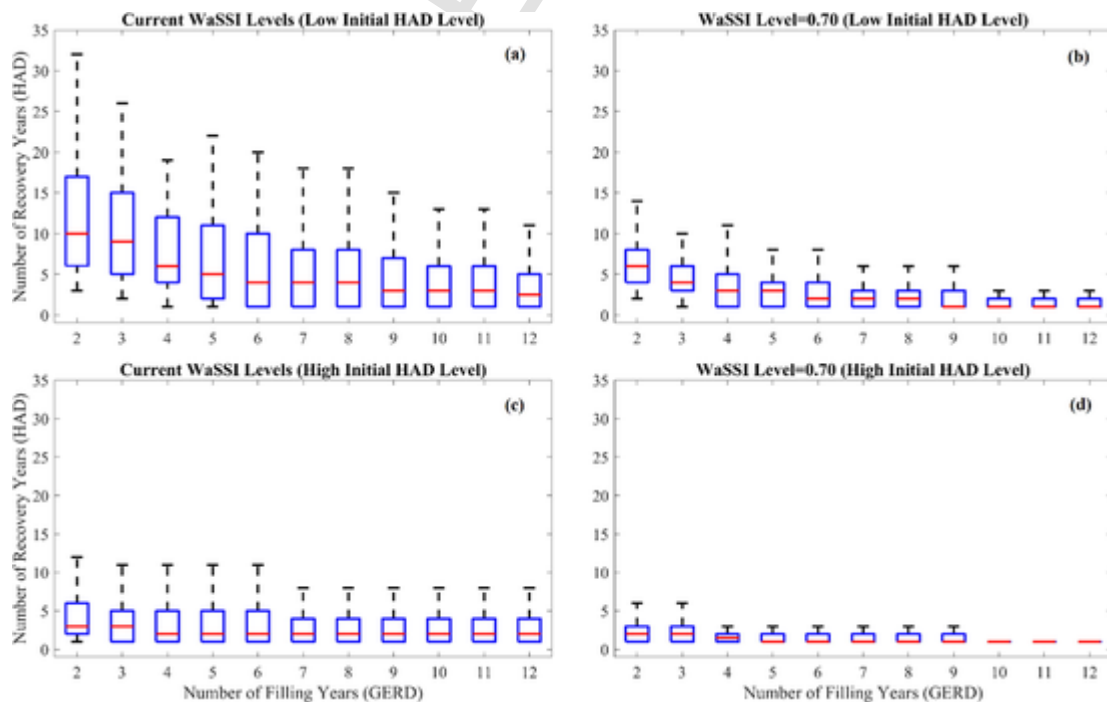


Fig. 12. The range of HAD recovery years under different GERD filling scenarios when assuming (a & c) current stress levels and (b & d) a predefined stress level ($WaSSI_{AG} = 0.70$). The upper and lower panels represent the scenarios of low and high initial HAD storage level, respectively.

to recover to its normal operation (175 m) and the less inflow reaching downstream after GERD operation.

Fig. 13 shows the changes in HAD operation after filling GERD considering both the recovery period of HAD and when reaching its normal operating level (only the results for the 3-year filling scenario with current stress conditions are shown in Fig. 13). The HAD operation was also compared to the historical HAD operation using a water balance model over the HAD reservoir with inputs from the satellite-based modeling developed by Eldardiry and Hossain (2019). As explained in the GERD operation (Fig. 10a), the Blue Nile flow downstream of GERD becomes more regulated and therefore alters the HAD inflow hydrograph. Compared to the historical maximum HAD inflow, higher inflows (with more than $3 \text{ km}^3/\text{month}$) are expected during the winter months (December through February). During the GERD storage months (or BNB rainy season; June through September), the HAD inflow is expected to drop with maximum reduction in August ($-7.6 \text{ km}^3/\text{month}$ and $-1.40 \text{ km}^3/\text{month}$ compared to historical average and minimum HAD inflow, respectively). The increase in winter months downstream flow (GERD outflow) maybe favored by Egypt as it will reduce losses due to evaporation in Lake Nasser at HAD dam. However, as indicated in Fig. 13b, reduction in annual evaporation can be significant only during the recovery period of HAD, i.e., when the HAD storage is below its normal levels. The annual evaporation losses are expected to decrease during the recovery period in a range between 11% (current stresses) and 7% ($\text{WaSSI}_{AG} = 0.70$) when operating after 3-year GERD filling scenario.

During HAD recovery from a 3-year filling scenario, HAD level will significantly drop down with a monthly average of 170.9 m (Fig. 13c) compared to an average historical HAD level of monthly average that equals to 175.6 m (about 4.7 m difference). The HAD levels above the historical minimum levels is noticed in all months (with an average of 1.3 m) except for October through December, where still the HAD operation is below the minimum historical levels. These months follow the rainy season in Ethiopia, and therefore this difference reveals the failure of the HAD to recover from the inflow deficit during the summer months where most of the water is stored in GERD. Adopting a higher stress level of 0.70 (Fig. S6 in Supplementary material) will elevate the water levels in the HAD since we allow for more stressed system downstream. Higher HAD storage levels is noticed for most of the year after the recovery period compared to historical average levels, which reflects an advantage of flow regulation by GERD operation (i.e., higher releases in the winter months). However, it is worth noting that reaching such higher levels will only be achieved after the recov-

ery period, which is driven by the initial HAD storage level, GERD filling scenario and the streamflow variability. Similarly, comparing the difference between the average monthly storage change of HAD (during GERD operation vs historical average), September and July experience the largest difference with a reduction of $-6.5 \text{ km}^3/\text{month}$ and $-3.9 \text{ km}^3/\text{month}$, respectively. The results of HAD operation underscores the existence of potential seasons where Egypt can employ more sustainable strategies to better manage the water especially in the months following the BNB rainy season.

5. Discussion

Our study presented a blueprint for the adaptation of HAD to upstream dams under various plausible scenarios, with focus on the GERD dam, currently under construction along the Blue Nile in Ethiopia. The results showed the importance of different decision factors when considering such a transboundary issue. In our analysis, we investigated four factors: GERD filling scenario (or number of years to completely fill the dam to its storage capacity), streamflow variability, HAD initial storage level, and downstream adaptation strategy. Challenges with operating HAD can be alleviated if riparian countries agree upon a coordinated operations of both reservoirs (GERD and HAD). While our analysis considered a unilateral decision for operations, a coordinated approach of operations would help in sharing benefits, particularly during low-flow or high-flow periods (Mulat and Moges, 2014; Taye et al., 2016). Whether the GERD will be filled through cooperation or through unilateral determination is a critical factor to consider when deciding an appropriate adaptation strategy. While Egypt would opt for a slow-paced filling scenario, e.g., 7 years or more as revealed in our analysis, filling in shorter periods would obviously impact the downstream water use and consequently the operation of HAD. Our results highlighted the opportunities to operate the HAD in a more prudent way that would store more water during the summer, in lieu of historically releasing water during the high flow season (June through September). In addition, preparing in advance for GERD filling by maintaining HAD storage at a high level can significantly mitigate the negative impacts of GERD filling. Such adaptation decisions can also benefit future HAD operation against other upstream dams. Sudan, for instance, has three planned dams (Shereik, Kajbar, and Dal dams) with a total hydropower capacity of more than 2000 MW. While these dams might operate in the future as only Run-of-the-River hydroelectric systems, HAD has to adapt its operation to expected reduction in the flow reaching downstream, primarily due to evaporation losses in the reservoirs formed by these dams. As demonstrated in our study, a trans-

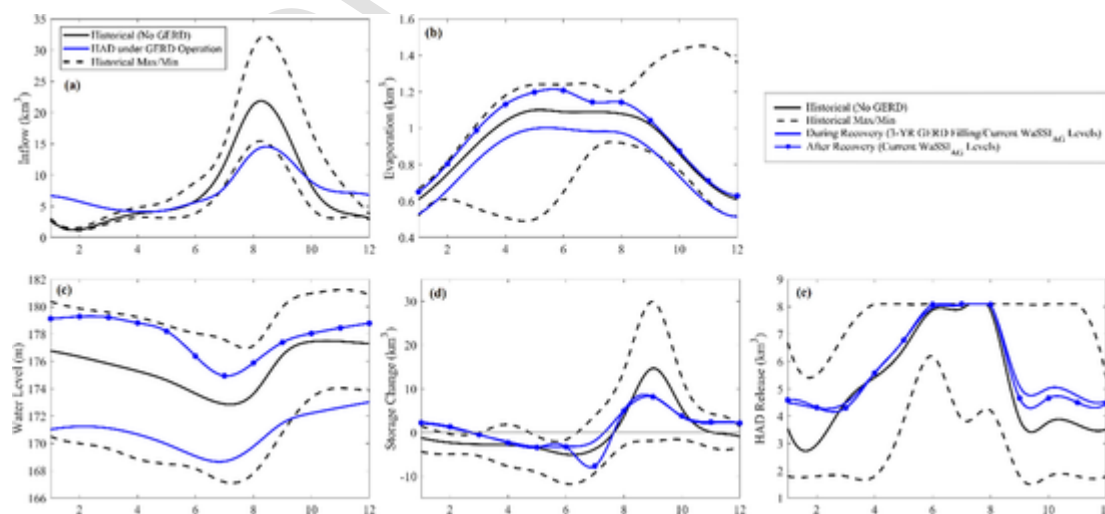


Fig. 13. Different hydrologic variables (inflow, evaporation, water level, storage change, and release) of the HAD operation during the GERD operation phase.

boundary issue is complicated by the different factors involved in making decision or finding an equitable solution amid riparian countries. While we tested different scenarios of HAD operation, future studies can further explore other decision factors including scenarios for irrigation water use in Sudan and Ethiopia. Thus, a multi-lateral negotiation is a compelling pathway to agree upon various decision factors that would guarantee the development plans of each riparian country.

Our optimal modeling of HAD operation resulted in more HAD releases than what currently released in winter months (from September to March). The higher releases are noticed in both filling and operation phases (Fig. 9a and 13e). This HAD optimal operation indicates that current operation of the dam doesn't exploit the hydropower capacity installed and only hydropower is assumed to be a by-product of the dam release. The lower production of hydropower in HAD is also affirmed by the World Bank statistics, which indicated a drop in the percentage of electricity produced from Hydropower in Egypt from 23.5% in 1990 to only 8% in 2014. This drop is attributed to the increase in power plants fueled by natural gas, which contributes more than 80% of the power generation in Egypt. The decision to optimize the HAD hydropower production or assume a by-product scenario provides another opportunity to HAD operators to control the HAD releases in periods with inflow reduction, as the case during the GERD filling. The integration of hydropower (energy sector) and irrigation (food sector) in our blueprint is important in addressing future challenges facing the Food, Energy, and Water (FEW) system across transboundary basins, e.g., Nile basin (Al-Saidi et al., 2017; Allam and Eltahir, 2019).

Taking advantage of globally free satellite observations at high spatial and temporal resolution makes our blueprint conceptually transferable to other transboundary basins as construction of mainstem and tributary dams becomes more widespread (Kalitsi, 2003; Sabo et al., 2017). For instance, more than 20 dams have been built by Turkey in the headwaters of the Euphrates river for hydropower and irrigation. Such dams impact downstream countries (Syria and Iraq) leading to reduced flow and potential desiccation with projected changes in climate (Zeitoun et al., 2013). Similarly, the case of damming the Lower Mekong River is spurring interest in South Asia to investigate how existing dams would operate to sustain the world's largest inland fishery (Hecht et al., 2019). Thus, harnessing the satellite information in transboundary basins of developing countries could provide a more effective and immediately actionable assessment of pre-existing dams operation under various scenarios of on-going or future dams.

6. Conclusion

The blueprint presented in our study explores the opportunities to adapt the operation of existing dams under the combined impacts of filling/operation of upstream planned dams and water demand in the downstream. Using the HAD-GERD dams as a typical paradigm of large hydropower dams (existing and planned) in a transboundary basin, we examined the impacts of different GERD scenarios on HAD operation. Our key findings can be summarized as follows:

1. The status quo stresses downstream of the HAD reveals a highly stressed system (average $WaSSI_{AG} = 0.95$) in winter months (November through March) due to water being used for irrigation with less releases from the HAD. The summer months (May through August) experience low stresses with an average of 0.50 when HAD empties its storage to prepare for the Blue Nile rainy season. The seasonal differences in the stresses downstream of the HAD reinforce the importance of considering opportunities to revisit the HAD operation in the summer months to mitigate the expected reduction in water supply during the GERD filling/operation phases.
2. The HAD dam will undergo different operational modes during the filling and operational phases of GERD. The filling scenarios of the

GERD dam indicated a smaller impacts on downstream outflow when following a slower filling scenario or by keeping HAD storage at high level prior to GERD filling. A 3-year filling scenario can lead to a significant declining trend in HAD water levels that would be slightly improved if higher stress level ($WaSSI_{AG} = 0.70$) are adopted in the summer months. On the other hand following a slower filling scenario, e.g., more than 7-year filling scenario, would lead to an average stabilized HAD levels.

3. The GERD operation will regulate the flow in the Blue Nile and therefore less intra-annual variability in the HAD inflow. When the GERD starts its operation (post-filling phase), the HAD will experience a recovery period to restore its storage to a normal operating level. Such recovery transition will depend on the filling scenario, climate conditions, HAD storage level when GERD starts filling, and the stress level employed downstream of the HAD. Our results concluded that under years of different climate (varies between dry and wet), the HAD would recover to its normal operation after an average of 7 and 3 years for 3- and 7-year filling scenarios, respectively. This period can significantly drop down if the initial HAD storage is kept at a higher level or by elevating downstream stresses in the summer (e.g., $WaSSI_{AG} = 0.70$).

As the GERD dam is a matter of fact, Egypt has to accept the fait accompli and explore adaptation strategies to face the expected reduction in Nile water supply. While adapting the HAD operation, as suggested in our results, is one approach to alleviate the GERD impacts, it becomes urgent for a populous country like Egypt, to think of alternative resources to support its development plans. For example, importing virtual water (water used in the production of any traded commodity) becomes an integral element in transboundary basin management. Zeitoun et al. (2010) estimated about 41 km³ of virtual water imported annually by the Nile basin states between 1998 and 2004. This additional water to the basin represents one third of the annual Nile flow and plays a key role in filling the freshwater deficits of downstream countries, Egypt and Sudan. Other alternative measures include, adopting water-efficient agricultural technologies like sprinkler and drip irrigation, building new desalination and water treatment plants, and imposing firm penalties on wasteful irrigation practices or unofficial use of irrigation water. Riparian countries of the Nile basin should agree upon a long-term framework that explicitly accounts for the impacts of future projects along the Nile. Such a framework should aspire to a win-win solution and consider equitable rights of development for all Nile countries.

7. Data availability statement

We have begun archiving our data in the platform Hydroshare supported by the CUASHI. Our archiving process is not yet complete, and we expect the archiving to be complete by January 2020. It should also be noted that most data and models used in this study are publicly available. The VIC hydrologic model is available from <https://vic.readthedocs.io/en/master/>. CHIRPS satellite precipitation data are available from <ftp://ftp.chg.ucsb.edu/pub/org/chg/products/CHIRPS-2.0>. Satellite data from Landsat mission is available from <https://landsatlook.usgs.gov/>. GLDAS outputs are available from <https://ldas.gsfc.nasa.gov/gldas> VIC model parameters and derived landcover maps and dam data are available from first author on request.

Uncited references

Block and Strzepek (2010), MALR (2014).

Declaration of Competing Interest

The authors declare that they have no known competing financial interests or personal relationships that could have appeared to influence the work reported in this paper.

Acknowledgement

This work was supported by NASA Applied Science Program grant in Water Resources NNX15AC63G and NNX16AQ54G (Program Manager Dr. Bradley Doorn). Additional support from University of Washington Global Affairs and the Ivanhoe Foundation are gratefully acknowledged.

Appendix A. Supplementary data

Supplementary data to this article can be found online at <https://doi.org/10.1016/j.jhydrol.2020.125708>.

References

- Abd-El Monsef, H., Smith, S.E., Darwish, K., 2015. Impacts of the Aswan high dam after 50 years. *Water Resour. Manage.* 29 (6), 1873–1885.
- Abteu, W., Dessu, S.B., 2019. The Grand Ethiopian Renaissance Dam on the Blue Nile. Springer International Publishing.
- Aljefri, Y.M., Fang, L., Hipel, K.W., Madani, K., 2019. Strategic analyses of the hydropolitical conflicts surrounding the grand ethiopian renaissance dam. *Group Decis. Negot.* 28 (2), 305–340. doi:10.1007/s10726-019-09612-x.
- Allam, M.M., Eltahir, E.A.B., 2019. Water-Energy-Food Nexus Sustainability in the Upper Blue Nile (UBN) Basin. *Front. Environ. Sci.* 7 (5).
- Allen, R.G., Tasumi, M., Trezza, R., 2007. Satellite-Based Energy Balance for Mapping Evapotranspiration with Internalized Calibration (METRIC) – Model. *J. Irrig. Drain Eng.* 133 (4), 380–394. doi:10.1061/(ASCE)0733-9437(2007)133:4(380).
- Al-Saidi, M., Elagib, N.A., Ribbe, L., Schellenberg, T., Roach, E., Ozhan, D., 2017. Water-energy-food security nexus in the eastern Nile basin: Assessing the potential of transboundary regional cooperation. *Water-Energy-Food Nexus: Principles and Practices* 229, 103.
- Bastiaanssen, W.G.M., Menenti, M., Feddes, R.A., Holtslag, A.A.M., 1998. A remote sensing surface energy balance algorithm for land (SEBAL). 1. Formulation. *J. Hydrol.* 212–213, 198–212. doi:10.1016/S0022-1694(98)00253-4.
- Bastiaanssen, W.G.M., Noordman, E.J.M., Pelgrum, H., Davids, G., Thoreson, B.P., Allen, R.G., 2005. SEBAL model with remotely sensed data to improve water-resources management under actual field conditions. *J. Irrig. Drain Eng.* 131 (1), 85–93. doi:10.1061/(ASCE)0733-9437(2005)131:1(85).
- Balthrop, C., & F. Hossain (2010). Short note: a review of state of the art on treaties in relation to management of transboundary flooding in international river basins and the global precipitation measurement mission. *Water Policy*, 12(5), 635.
- Basheer, M., Wheeler, K.G., Elagib, N.A., Etichia, M., Zagana, E.A., Abdo, G.M., Harou, J.J., 2020. Filling Africa's largest hydropower dam should consider engineering realities. *One Earth* 3 (3), 277–281. doi:10.1016/j.oneear.2020.08.015.
- Block, P., Strzepek, K., 2010. Economic analysis of large-scale upstream river basin development on the blue Nile in Ethiopia considering transient conditions, climate variability, and climate change. *J. Water Resour. Plann. Manage.* 136 (2), 156–166. doi:10.1061/(ASCE)WR.1943-5452.0000022.
- Borrok, D.M., Chen, J., Eldardiry, H., Habib, E., 2018. A framework for incorporating the impact of water quality on water supply stress: an example from Louisiana, USA. *J. Am. Water Resour. Assoc.* 54 (1), 134–147. doi:10.1111/1752-1688.12597.
- Bonnema, M. and F. Hossain (2020) Assessing the Potential of the Surface Water and Ocean Topography Mission for Reservoir Monitoring in the Mekong River Basin. *Water Resources Research*, vol. 55(1), pp. 444-461 (doi:10.1029/2018WR023743).
- Bonnema, M., Hossain, F., 2017. Inferring reservoir operating patterns across the Mekong Basin using only space observations. *Water Resour. Res.* 53 (5), 3791–3810. doi:10.1002/2016WR019978.
- CAPMAS, E. (2014). Annual Bulletin of Statistical Crop Area and Plant Production. The central agency for public mobilisation and statistics.
- Cascão, Ana Elisa, Nicol, Alan, 2016. GERD: new norms of cooperation in the Nile Basin? *Water Int.* 41 (4), 550–573. doi:10.1080/02508060.2016.1180763.
- Conway, Declan, 2017. Future Nile river flows. *Nature Clim Change* 7 (5), 319–320. doi:10.1038/nclimate3285.
- Crétaux, J.-F., Jelinski, W., Calmant, S., Kouraev, A., Vuglinski, V., Bergé-Nguyen, M., Gennero, M.-C., Nino, F., Abarca Del Rio, R., Cazenave, A., Maisongrande, P., 2011. SOLS: A lake database to monitor in the Near Real Time water level and storage variations from remote sensing data. *Adv. Space Res.* 47 (9), 1497–1507. doi:10.1016/j.asr.2011.01.004.
- Decker, M., Brunke, M. A., Wang, Z., Sakaguchi, K., Zeng, X., & Bosilovich, M. G. (2012). Evaluation of the reanalysis products from GSFC, NCEP, and ECMWF using flux tower observations. *Journal of Climate*, 25(6), 1916-1944.
- Digna, Reem F., Mohamed, Yasir A., van der Zaag, Pieter, Uhlenbrook, Stefan, van der Krogt, Wil, Corzo, Gerald, 2018. Impact of water resources development on water availability for hydropower production and irrigated agriculture of the eastern Nile Basin. *J. Water Resour. Plann. Manage.* 144 (5), 05018007. doi:10.1061/(ASCE)WR.1943-5452.0000912.
- Bastawesy, Mohammed El, 2015. Hydrological scenarios of the renaissance dam in Ethiopia and its hydro-environmental impact on the Nile downstream. *J. Hydrol. Eng.* 20 (7), 04014083. doi:10.1061/(ASCE)HE.1943-5584.0001112.
- Eldardiry, Hisham, Habib, Emad, Borrok, David M, 2016. Small-scale catchment analysis of water stress in wet regions of the U.S.: An example from Louisiana. *Environ. Res. Lett.* 11 (12), 124031. doi:10.1088/1748-9326/aa51dc.
- Eldardiry, H., & Hossain, F. (2019). Understanding Reservoir Operating Rules in the Trans-boundary Nile River Basin Using Macroscale Hydrologic Modeling with Satellite Measurements. *Journal of Hydrometeorology*, 20(11), 2253-2269.
- Elnmer, Ayat, Khadr, Mosaad, Kanae, Shinjiro, Tawfik, Ahmed, 2019. Mapping daily and seasonally evapotranspiration using remote sensing techniques over the Nile delta. *Agric. Water Manag.* 213, 682–692. doi:10.1016/j.agwat.2018.11.009.
- El-Shabrawy, G.M., 2009. Lake Nasser—Nubia. In: *The Nile*. Springer, Dordrecht, pp. 125–155.
- Falkenmark, M., 1989. The massive water scarcity now threatening Africa: Why isn't it being addressed? *Ambio* 112–118.
- Famiglietti, J.S., Cazenave, A., Eicker, A., Reager, J.T., Rodell, M., Velicogna, I., 2015. Satellites provide the big picture. *Science* 349 (6249), 684–685.
- FAO AQUASTAT database, Irrigation and Drainage Retrieved from: <http://www.fao.org/nr/water/aquastat/irrigationdrainage/index.stm>, Accessed 29 OCT20182016
- Fisher, Joshua B., Melton, Forrest, Middleton, Elizabeth, Hain, Christopher, Anderson, Martha, Allen, Richard, McCabe, Matthew F., Hook, Simon, Baldocchi, Dennis, Townsend, Philip A., Kilic, Ayse, Tu, Kevin, Miralles, Diego D., Perret, Johan, Lagouarde, Jean-Pierre, Waliser, Duane, Purdy, Adam J., French, Andrew, Schimel, David, Famiglietti, James S., Stephens, Graeme, Wood, Eric F., 2017. The future of evapotranspiration: Global requirements for ecosystem functioning, carbon and climate feedbacks, agricultural management, and water resources. *Water Resour. Res.* 53 (4), 2618–2626. doi:10.1002/2016WR020175.
- Georgakakos, A.P., Yao, H., Kistenmacher, M., Georgakakos, K.P., Graham, N.E., Cheng, F.-Y., Spencer, C., Shamir, E., 2012. Value of adaptive water resources management in Northern California under climatic variability and change: Reservoir management. *J. Hydrol.* 412–413, 34–46. doi:10.1016/j.jhydrol.2011.04.038.
- Gouda, Dalia M. (Ed.), 2016. Social Capital and Local Water Management in Egypt Social Capital and Local Water Management in Egypt. American University in Cairo Press.
- Grumbine, R Edward, Dore, John, Xu, Jianchu, 2012. Mekong hydropower: Drivers of change and governance challenges. *Front. Ecol. Environ.* 10 (2), 91–98. doi:10.1890/110146.
- Grumbine, R.E., Xu, J., 2011. Mekong hydropower development. *Science* 332 (6026), 178–179.
- Hecht, Jory S., Lacombe, Guillaume, Arias, Mauricio E., Dang, Thanh Duc, Piman, Thanop, 2019. Hydropower dams of the Mekong River basin: A review of their hydrological impacts. *J. Hydrol.* 568, 285–300. doi:10.1016/j.jhydrol.2018.10.045.
- Hossain, Faisal, Katiyar, Nitin, Hong, Yang, Wolf, Aaron, 2007. The emerging role of satellite rainfall data in improving the hydro-political situation of flood monitoring in the under-developed regions of the world. *Nat. Hazards* 43 (2), 199–210. doi:10.1007/s11069-006-9094-x.
- Husr, H.E., Black, R.P., Simaika, Y.M., 1966. The major Nile projects. Nile control department – Ministry Of Public Works. Nile Basin Encyclopedia 10.
- Ji, L., Senay, G. B., & Verdin, J. P. (2015). Evaluation of the Global Land Data Assimilation System (GLDAS) air temperature data products. *Journal of Hydrometeorology*, 16(6), 2463-2480.
- Kalitsi, E. A. K. (2003). Problems and prospects for hydropower development in Africa. In *The Workshop for African Energy Experts on Operationalizing the NIGPAD Energy Initiative* (pp. 2-4).
- Karamouz, Mohammad, Houck, Mark H., 1982. Annual and monthly reservoir operating rules generated by deterministic optimization. *Water Resour. Res.* 18 (5), 1337–1344. doi:10.1029/WR018i05p01337.
- Kibaroglu, Aysegül, Gürsoy, Sezin İba, 2015. Water–energy–food nexus in a transboundary context: The Euphrates–Tigris river basin as a case study. *Water Int.* 40 (5–6), 824–838. doi:10.1080/02508060.2015.1078577.
- King, A., Block, P., 2014. An assessment of reservoir filling policies for the Grand Ethiopian Renaissance Dam. *J. Water Clim. Change* 5 (2), 233–243.
- Kummu, M., Gerten, D., Heinke, J., Konzmann, M., Varis, O., 2014. Climate-driven interannual variability of water scarcity in food production potential: A global analysis. *Hydrol. Earth Syst. Sci.* 18 (2), 447–461.
- Lehner, B., Liermann, C.R., Revenga, C., Vörösmarty, C., Fekete, B., Crouzet, P., et al., 2011. High-resolution mapping of the world's reservoirs and dams for sustainable river-flow management. *Front. Ecol. Environ.* 9 (9), 494–502.
- Lettenmaier, D.P., Alsdorf, D., Dozier, J., Huffman, G.J., Pan, M., Wood, E.F., 2015. Inroads of remote sensing into hydrologic science during the WRR era. *Water Resour. Res.* 51 (9), 7309–7342.
- Liou, Y.A., Kar, S.K., 2014. Evapotranspiration estimation with remote sensing and various surface energy balance algorithms – A review. *Energies* 7 (5), 2821–2849.
- MALR, 2014. The ministry of agriculture and land reclamation, Annual bulletin of indicators of agricultural statistics.
- Melesse, A.M., Abteu, W., Setegn, S.G., Dessalegne, T., 2011. Hydrological variability and climate of the Upper Blue Nile River basin. *Nile River Basin*. Springer, Dordrecht, pp. 3–37.
- MIT, 2014. The Grand Ethiopian Renaissance Dam: An opportunity for collaboration and shared benefits in the Eastern Nile Basin: An amicus brief to the Riparian Nations of Ethiopia, Sudan and Egypt from the international, non-partisan Eastern Nile working group. Massachusetts Institute of Technology, Boston.
- Molden, D.J., Awulachew, S.B., Conniff, K., Rebelo, L.M., Mohamed, Y., Peden, D.G., et al., 2009. Nile Basin Focal Project. Synthesis report.
- Moussa, A.M.A., 2018. Dynamic operation rules of multi-purpose reservoir for better flood management. *Alexandria Eng. J.* 57 (3), 1665–1679.

- Mulat, A.G., Moges, S.A., 2014. Assessment of the impact of the Grand Ethiopian Renaissance Dam on the performance of the High Aswan Dam. *J. Water Resour. Protect.* 6 (6), 583.
- Mulligan, M., van Soesbergen, A., Sáenz, L., 2020. GOODD, a global dataset of more than 38,000 georeferenced dams. *Sci. Data* 7 (1), 1–8.
- Munia, H., Guillaume, J.H.A., Mirumachi, N., Porkka, M., Wada, Y., Kumm, M., 2016. Water stress in global transboundary river basins: Significance of upstream water use on downstream stress. *Environ. Res. Lett.* 11 (1), 014002.
- Pahl-Wostl, C., 2007. Transitions towards adaptive management of water facing climate and global change. *Water Resour. Manage.* 21 (1), 49–62.
- Paisley, R.K., Henshaw, T.W., 2013. Transboundary governance of the Nile River Basin: Past, present and future. *Environ. Develop.* 7, 59–71.
- Rahman, M.A., 2013. Water security: Ethiopia-Egypt transboundary challenges over the Nile river basin. *J. Asian Afr. Stud.* 48 (1), 35–46.
- Rodell, M., Houser, P.R., Jambor, U.E.A., Gottschalk, J., Mitchell, K., Meng, C.J., Entin, J.K., 2004. The global land data assimilation system. *Bull. Am. Meteorol. Soc.* 85 (3), 381–394.
- Sabo, J.L., Ruhi, A., Holtgrieve, G.W., Elliott, V., Arias, M.E., Ngor, P.B., et al., 2017. Designing river flows to improve food security futures in the Lower Mekong Basin. *Science* 358 (6368), eaao1053.
- Senay, G.B., Friedrichs, M., Singh, R.K., Velpuri, N.M., 2016. Evaluating Landsat 8 evapotranspiration for water use mapping in the Colorado River Basin. *Remote Sens. Environ.* 185, 171–185.
- Siam, M.S., Eltahir, E.A., 2017. Climate change enhances interannual variability of the Nile river flow. *Nat. Clim. Change* 7 (5), 350–354.
- Sheffield, J., Wood, E.F., Pan, M., Beck, H., Coccia, G., Serrat-Capdevila, A., Verbist, K., 2018. Satellite remote sensing for water resources management: potential for supporting sustainable development in data-poor regions. *Water Resour. Res.* 54 (12), 9724–9758.
- Sun, G., McNulty, S.G., Moore Myers, J.A., Cohen, E.C., 2008. Impacts of multiple stresses on water demand and supply across the Southeastern United States. *J. Am. Water Resour. Assoc.* 44 (6), 1441–1457.
- Taye, M.T., Tadesse, T., Senay, G.B., Block, P., 2016. The grand Ethiopian renaissance dam: source of cooperation or contention? *J. Water Resour. Plann. Manage.* 142 (11), 02516001.
- Thomas, H.A., Jr., Revelle, R., 1966. On the efficient use of High Aswan Dam for hydropower and irrigation. *Manage. Sci.* 12 (8), B-296.
- USBR, 1964. Land and Water Resources of the Blue Nile Basin. Ethiopia, United States Department of the Interior, Bureau of Reclamation.
- Vörösmarty, C.J., Green, P., Salisbury, J., Lammers, R.B., 2000. Global water resources: Vulnerability from climate change and population growth. *Science* 289 (5477), 284–288.
- Wada, Y., Bierkens, M.F., 2014. Sustainability of global water use: Past reconstruction and future projections. *Environ. Res. Lett.* 9 (10), 104003.
- Wheeler, K.G., Basheer, M., Mekonnen, Z.T., Eltoun, S.O., Mersha, A., Abdo, G.M., et al., 2016. Cooperative filling approaches for the grand Ethiopian renaissance dam. *Water Int.* 41 (4), 611–634.
- Wheeler, K.G., Hall, J.W., Abdo, G.M., Dadson, S.J., Kasprzyk, J.R., Smith, R., Zagana, E.A., 2018. Exploring cooperative transboundary river management strategies for the Eastern Nile Basin. *Water Resour. Res.* 54 (11), 9224–9254.
- Whittington, D., Waterbury, J., Jeuland, M., 2014. The grand renaissance dam and prospects for cooperation on the eastern Nile. *Water Policy* 16 (4), 595–608.
- Zarfl, C., Lumsdon, A.E., Berlekamp, J., Tydecks, L., Tockner, K., 2015. A global boom in hydropower dam construction. *Aquat. Sci.* 77 (1), 161–170.
- Zeitoun, M., Goulden, M., Tickner, D., 2013. Current and future challenges facing transboundary river basin management. *WIREs Climate Change* 4 (5), 331–349.
- Zeitoun, M., Allan, J.T., Mohielden, Y., 2010. Virtual water ‘flows’ of the Nile Basin, 1998–2004: A first approximation and implications for water security. *Global Environ. Change* 20 (2), 229–242.
- Zhang, Y., Block, P., Hammond, M., King, A., 2015. Ethiopia’s Grand Renaissance Dam: Implications for downstream riparian countries. *J. Water Resour. Plann. Manage.* 141 (9), 05015002.
- Zhang, W., Liu, P., Wang, H., Chen, J., Lei, X., Feng, M., 2017. Reservoir adaptive operating rules based on both of historical streamflow and future projections. *J. Hydrol.* 553, 691–707.
- Zhou, T., Voisin, N., Leng, G., Huang, M., Kraucunas, I., 2018. Sensitivity of regulated flow regimes to climate change in the western United States. *J. Hydrometeorol.* 19 (3), 499–515.